Nanoripple formation on TiO_2(110) by low-energy grazing incidence ion sputtering

Tim Luttrell and Matthias Batzill
Department of Physics, University of South Florida, Tampa, Florida 33620, USA
(Received 22 April 2010; revised manuscript received 15 June 2010; published 8 July 2010)

The self-formation of metastable nanoripples by low-energy Ar^+ ions impacting at a grazing incidence angle on a TiO_2(110) surface has been investigated by scanning tunneling microscopy. Ripple formation is a consequence of preferential sputtering of monatomic step edges with a directional component perpendicular to the ion-beam azimuth. The combination of preferential erosion of step edges and ion-beam-induced surface roughening results in a surface morphology with nanoripples aligned parallel to the ion-beam azimuth. We investigate the surface-structure evolution as a function of ion fluence for two ion-beam azimuth directions. Analysis of the formation and evolution of sputter-induced vacancy islands shows that under the conditions employed here (0.8 keV Ar ions, 8° grazing incidence angle) the sputter probability at step edges is significantly enhanced compared to sputtering at flat terraces. Although the initial vacancy island morphology can be strongly influenced by the step-edge formation energies for different crystallographic orientations, both investigated azimuth directions form similar ripple structures at high ion fluences. This study demonstrates that grazing incidence ion beams can be employed to pattern oxide substrates with quasiperiodic nanoripples with ripple spacing of tens of nanometer.

DOI: 10.1103/PhysRevB.82.035408 PACS number(s): 79.20.Rf, 68.47.Gh, 68.37.Ef

I. INTRODUCTION

Patterning of surfaces with nanostructures can modify their chemical and physical properties. Furthermore, nanostructuring of thin-film substrates will affect film growth[1,2] and may enable relaxation of lattice misfits in heterostructures.[3,4] In addition, by patterning the surface with lateral anisotropic features, such as ripples, films with artificial anisotropic properties can be grown. Large-scale patterning of surfaces with feature sizes in the ~10 nm range requires self-formation mechanisms. Here we discuss the use of low-energy, grazing-incidence ion beams for patterning single-crystal surfaces with nanoripple structures. Sputtering by low-energy ions can be applied to a wide range of materials and thus the mechanisms discussed here may be applied to many single-crystal substrates. The material used in this study is a rutile-TiO_2(110) wafer, as a model system for transition-metal oxides, an important class of materials for thin-film substrates.

Ion-sputtering-induced surface instabilities can result in nanostructure formation at surfaces. Two fundamentally different ion irradiation regimes can be distinguished: (i) ions impinging at the surface at incidence angles and ion energies large enough to penetrate the surface layer causing collision cascades in the subsurface region which subsequently result in ejection of surface atoms and (ii) grazing incidence ion irradiation, where the surface normal kinetic energy of the ions is too small to penetrate the surface layer and thus most ions are reflected form the surface, introducing only few defects at atomically flat terraces. The first regime has been studied extensively and it is understood that under these conditions the sputter yield becomes dependent on the surface curvature and this causes ripple formation[5–8] or other nanostructures such as quantum dots.[9] With increasing ion-incident angle (measured from the surface normal) the sputter yield initially increases because the ion energy is deposited closer to the surface and thus collision cascades cause the ejection of more surface atoms.[10] As the ion incident angle approaches a grazing angle the sputter yield decreases sharply due to the fact that the incoming ions cannot penetrate the surface layer anymore and are reflected from the surface.[11,12]

Furthermore, for low-energy ions the momentum transfer to the surface during the reflection is too small to induce lattice defects. This is the grazing incidence regime which is the focus of this paper. Compared to (close to) normal incidence ion bombardment, grazing incidence ion beams have been studied less by the scientific and engineering community. Recent studies, however, have demonstrated the utility of grazing incidence sputtering in surface "polishing"[13] and aiding alignment of molecules.[14] It has also been shown that irradiation of a single-crystal surface with grazing incidence ions results in the formation of nanoscale ripple structures parallel to the projection of the ion-beam direction on the surface.[15–17] The formation mechanism of this ripple structure is fundamentally different from the ripple formation at nonglancing angles. At glancing angle the ripple formation is a consequence of higher sputter yields at monatomic step edges compared to atomically flat terraces.[18,19] Consequently, it has been shown that step edges parallel to the ion beam are stabilized while step edges that have a directional component perpendicular to the ion-beam azimuth are preferentially eroded.[20] This results in step arrays parallel to the beam and subsequent formation of ripples whose separation tend to increase with irradiation duration.[21]

The studies reported here on TiO_2 are the first studies of this kind on a metal oxide. Previous studies of structure formation by grazing ion beams concentrated on metal surfaces[17–19,21,22] and ionic crystals such as CaF_2(111)[15,16] and KBr(001).[23] While the studies on Pt(111) by the Michely group are comprehensive, the main question this present study addresses is if the same processes are applicable to more complex materials such as covalent/ionic bonded oxides, i.e., materials for which single-crystal wafers have potential applications, such as thin-film substrates.

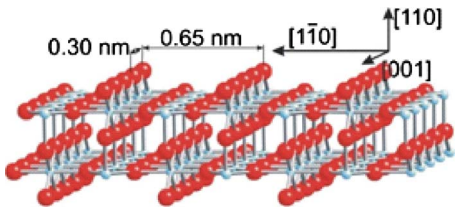

FIG. 1. (Color online) Ball-and-stick model of TiO_2(110) surface.

Prior to the investigation of structure formation due to ion sputtering, ion-scattering experiments of grazing incident ions on metal single-crystal surfaces have shown that the (quasielastic) reflection of the ion beam depends on the surface crystallographic orientation, i.e., the azimuth incident angle of the ion beam relative to low-index crystallographic surface directions.[24–27]

For low-index crystallographic directions a higher ion-beam reflection has been observed which was attributed to surface channeling. This demonstrates that grazing incident ions interact differently in surface-channeling and nonchanneling directions and consequently a difference in surface sputtering events may be expected in addition to sputtering at step edges and other surface defects. Furthermore, investigations of step-edge sputter yields on metal surfaces have indicated that subsurface ion channeling affects the sputter yield.[17] More open step-edge structures exhibit a lower sputter yield and incident ions may channel between the surface and the second atomic layer for low-index azimuth directions.

Metal oxides are more complex in their surface structure than metals and therefore a more pronounced directional dependence may be expected. Also, preferential sputtering of oxygen can change the surface composition. In the particular case of TiO_2 a surface reduction is known to trigger a (local) surface reconstruction[28] which may affect the ion-surface interaction. Therefore some TiO_2 specific properties need to be taken into account which is briefly discussed next.

II. STRUCTURAL CONSIDERATION OF THE TiO_2(110) surface for grazing incidence ion scattering

Rutile TiO_2(110) is the best studied transition-metal oxide surface[26] and thus a wealth of details regarding its properties is known. In this section a brief summary of some surface phenomena of this system relevant for this study are given.

Figure 1 shows a model of the surface structure of TiO_2(110). The (110) surface exhibits twofold coordinated bridging oxygen atoms that protrude from the surface plane and are closely spaced (0.30 nm) along the ⟨001⟩ direction and are far apart (0.65 nm) along the ⟨1$\bar{1}$0⟩ direction. This gives the surface a large corrugation and a strong structural anisotropy. This structural characteristic of the TiO_2(110) surface has implications for grazing incidence ion bombardment. Ions impinging at the surface are deflected through Coulomb interactions between the atom cores giving rise to a shadow cone behind the scatter atom in which no ions can penetrate. The size and shape of this shadow cone has been discussed extensively[29] for applications in structural determination of surfaces by low-energy ion scattering spectroscopy. A shadow cone of 0.8 keV Ar^+ ions incident at 8° grazing angle and interacting with surface oxygen anions extends ~2 nm behind the scatterer before the cone intersects the surface plane. It is apparent that under these conditions a bridging oxygen atom is lying within the shadow cone of its neighbor atom in the direction of the ion beam for both azimuths and therefore forming an envelope that prevents direct head-on ion impact on the surface atoms. This is the reason for the strongly reduced sputter yield at grazing incidence conditions. The shadow cone extends in three dimensions so that the in-plane shape of the shadow cone also needs to be considered. In the ⟨001⟩ direction, the rows of bridging oxygen atoms are farther apart and the oxygen atoms are closer spaced. This provides a better ion channeling than along the ⟨1$\bar{1}$0⟩ direction. From these arguments a smaller *terrace sputter* yield for the ⟨001⟩ azimuth compared to the ⟨1$\bar{1}$0⟩ direction may be anticipated. However, a more detailed binary collision simulation would be needed for a thorough theoretical analysis.

At step edges, surface atoms are not "protected" by the shadow-cone envelope and therefore direct ion impact results in higher sputtering rates. In addition, ions reflected from the lower terrace onto the step-edge atoms may also cause sputter events at steps. Therefore step-edge atoms are expected to experience a much higher sputter yield under grazing incidence conditions compared to terrace atoms. Comparing the crystal structure along ⟨001⟩ and ⟨1$\bar{1}$0⟩ directions gives information about the atom densities for step edges along these directions, which is expected to correlate with the sputter yield. Both directions exhibit open structures with cations and anions aligning in columns perpendicular to the planes. The density of anion and cation columns gives a rough measure for the expected step-edge sputter yield differences for the two azimuth directions with denser packed step edges having a higher ion-impact probability compared to more open structures. For the ⟨1$\bar{1}$0⟩ step orientation the column density is 28.4 atoms/nm^2 while for the ⟨001⟩ step orientation the column density is 41 atoms/nm^2. Thus this simple estimate suggests a 1.4 times higher step-edge sputter yield for grazing ions impinging on the ⟨001⟩-oriented steps, i.e., for ion beams along the ⟨1$\bar{1}$0⟩ azimuth, than for the ⟨1$\bar{1}$0⟩-oriented steps, i.e., for an ion-beam azimuth along the ⟨001⟩ crystallographic direction.

In addition to the bulk-truncated surface and step edges, the TiO_2(110) surface may also exhibit local 1×2 reconstructions. This surface reconstruction forms on TiO_2(110) if it is reduced. From TRIM simulations[30] an about four times higher sputter yield for the lighter O atoms compared to Ti atoms is calculated. Therefore oxygen is preferentially sputtered and the sample is reduced during ion irradiation. Thus regions of high sputtering, e.g., along step edges the surface may be prone to form this 1×2 reconstruction. This structural change, in turn, will affect the ion-beam interaction at step edges. Although the exact structure of the 1×2 reconstruction is controversial, a recent high-resolution, cross-sectional transmission electron microscopy study[31] has visu-

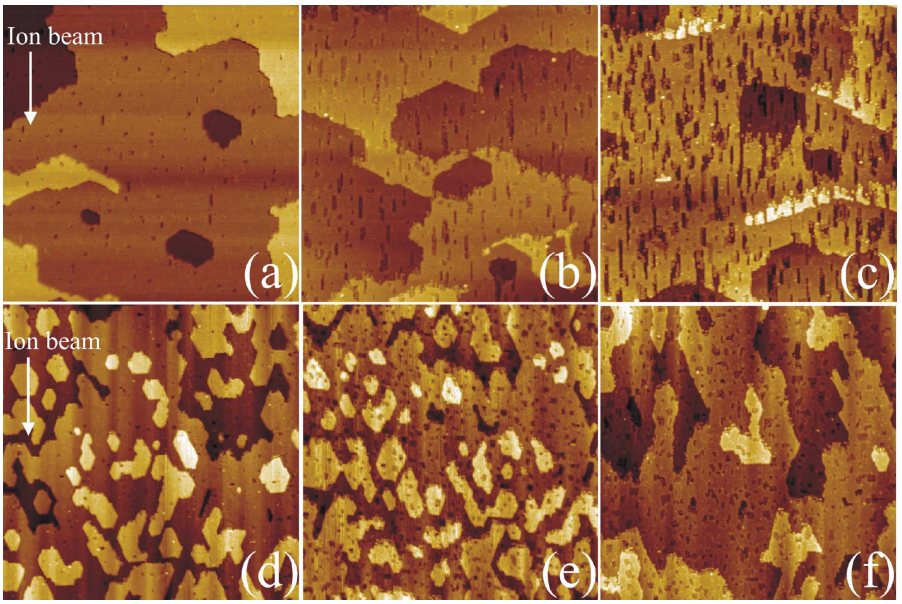

FIG. 2. (Color online) Shown are 200×200 nm^2 STM images of TiO_2(110) after grazing incidence irradiation along the ⟨001⟩ azimuth for (a) 20 min, (b) 80 min, and (c) 160 min and along the ⟨1$\bar{1}$0⟩ azimuth for (d) 5 min, (e) 20 min, and (f) 30 min.

alized Ti-interstitial atoms in *ih* octahedral sites.[32] This implies that the otherwise open channels along ⟨001⟩ and ⟨1$\bar{1}$0⟩ directions are (partially) blocked by the Ti-interstitial atoms in the 1×2 reconstructed phase. This should result in an increased step-edge sputtering compared to the unreconstructed surface, but should affect both azimuths in a similar manner.

Here we report experimental studies that verify the increased step-edge sputtering on TiO_2(110) surfaces under grazing incidence ion bombardment and show that the higher sputter yield at step edges is responsible for nanoripple formation at the surface. We compare nanoripple formation with the ion-beam azimuth direction aligned along the ⟨001⟩ and the ⟨1$\bar{1}$0⟩ azimuths.

III. EXPERIMENTAL METHODS

All the experiments were performed in an UHV chamber with a base pressure in the low 10^{-10} Torr range. The chamber was equipped with an Omicron variable temperature scanning tunnel microscope (STM), a commercial ion sputter gun (LK technologies), and a sample manipulator that allowed polar rotation relative to the ion gun. For change in the azimuthal orientation, the sample had to be removed from the vacuum chamber and remounted onto the sample plate. The azimuthal orientation of the sample relative to the ion beam was judged to be better than $\pm3°$. All the measurements shown here were taken at a polar incidence angle of 82°, i.e., 8° glancing angle. In addition the sample temperature, ion energy, and ion flux was kept constant at 400 °C, 800 eV, 1.3×10^7 ions/(m$^2\times$s), respectively. The elevated sample temperature during irradiation is necessary to provide enough thermal energy to heal sputter defects and to reform a crystalline, stoichiometric surface.[33] On the other hand the sample temperature was chosen low enough to avoid large-scale reorganization of the surface.

The rutile TiO_2(110) single crystal was obtain from MTI Corporation and was epipolished. The crystal was cleaned *in situ* by repeated Ar sputtering and annealing (700 °C) cycles.

IV. RESULTS

STM images of the surface evolution for short sputter times (low ion fluence) with irradiation along the ⟨001⟩ and the ⟨1$\bar{1}$0⟩ azimuths are shown in Fig. 2. Sputter-induced vacancies agglomerate and excess Ti dissolves into the bulk forming vacancy islands at the surface. Initially at low fluences the density of these vacancy islands increases until they coalesce to form larger islands. Comparing the two azimuths shows that surfaces irradiated along the ⟨1$\bar{1}$0⟩ direction exhibits a higher density of vacancy islands at low fluences compared to the ⟨001⟩ azimuth direction. This behavior can be more clearly seen in Fig. 3(a) which shows a plot of the island density versus sputter time. For both ion-beam directions the vacancy-island density increases at first and then drops off at longer sputter times as the individual islands merge. Also the shape of the islands is distinctively different for the two irradiation directions. It is obvious from visual inspection of the Fig. 2 that for the ion beam directed along the ⟨001⟩ azimuth the vacancy islands are elongated in the ⟨001⟩ direction, while for irradiation along the ⟨1$\bar{1}$0⟩ direction there is no obvious anisotropy of the vacancy island shape for low ion fluences. The differences in the aspect ratios of the vacancy islands can be obtained by plotting the total width of all islands, i.e., the sum of the width of all the vacancy islands in a 200×200 nm^2 STM image, against the summed lengths of all islands. This is shown in Fig. 3(b). In this plot the length and width are measured parallel and perpendicular to the ion-beam direction, respectively. The different data points in Fig. 3(b) are obtained for different sputter times. From a linear regression through these data points it can be seen that for the ⟨1$\bar{1}$0⟩ azimuth the islands grow almost uniformly in width and length while for the ⟨001⟩ azimuth the length of the islands are on average more than twice their width.

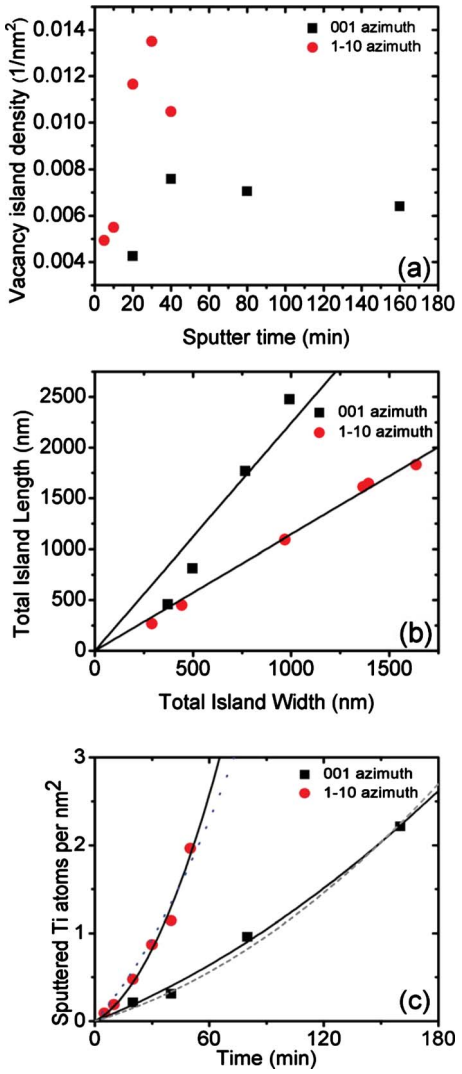

FIG. 3. (Color online) STM image analyses for surface properties as a function of sputter time for ion beams directed along the ⟨001⟩ (square symbols) and the ⟨1$\bar{1}$0⟩ azimuths (round symbols). (a) Shows the evolution of the vacancy island density with sputter time. (b) Shows the total island lengths versus widths. Each data point corresponds to a different sputter time. The total number of sputtered atoms derived from the total vacancy island area as a function of sputter time is shown in (c). The solid lines in (c) are the best quadratic fit to the data points while the dashed lines are fits restricting the linear term by predefined terrace sputter yields (see text).

To evaluate the sputter yield, the number of sputtered surface atoms per unit area, measured from the size of the vacancy islands, is plotted versus the sputter time (ion fluence). This is shown in Fig. 3(c) for the two azimuths directions. This plot shows an increase in the rate of sputtered atoms, i.e., the sputter yield is increasing with sputter time. Such a behavior is expected if the sputtering yield is larger at step edges than on terraces. In this case the total sputter yield from the surface is increasing as the step-edge density increases, i.e., as the surface becomes rougher. Therefore the increase in sputter yield with increased step-edge density, or vacancy-island density, is a direct verification for the higher sputter yield at step edges. Furthermore, Fig. 3(c) shows a larger sputter yield for the ⟨1$\bar{1}$0⟩ azimuth compared to the ⟨001⟩ azimuth direction. This directional dependence in the sputter yield was expected from the strongly anisotropic surface structure of the TiO_2(110) surface and may be attributed to variations in the terrace sputter yield for the two azimuth directions.

The higher sputter yield at step edges exposed to the ion beam compared to the sputter yield at terraces or steps oriented parallel to the beam can also be clearly appreciated from the structure of pre-existing step edges after ion irradiation. Figure 4(a) shows an STM image after 80 min irradiation. Step edges exposed to the ion beam (ascending steps) are much more "rugged" than steps parallel to the ion beam or descending steps. Although we cannot measure how much of the step edge was eroded by the ion beam the roughening of the step is a clear indication of stochastic removal of atoms by sputtering of the exposed step edge. In addition, the formation of 1×2 reconstruction strands is observed along these exposed step edges and within newly formed vacancy islands. This is evidence for the preferential O sputtering at step edges, which causes a local enrichment with Ti interstitials and consequently the formation of the reconstruction. This can be seen in Fig. 4(b). Thus the localization of 1×2 reconstruction strands close to step edges indicates the reduction in titania by preferential O sputtering from step edges and thus is an additional confirmation of the higher sputter yield at step edges compared to terraces.

Anisotropic structure formation as observed for grazing incidence ion irradiation along the ⟨001⟩ azimuth could also be partially influenced by a strong anisotropic diffusion of ion-beam-induced vacancies. To exclude this possibility we examine the vacancy island formation at normal incidence sputtering. If anisotropic diffusion was to contribute to the elongated vacancy island shape then some elongation of vacancy islands should be observable independent of the ion-beam direction. Figure 4(c) shows a surface bombarded with normal incidence ions but otherwise identical conditions as for the grazing incident experiments. The vacancy islands that formed do not exhibit any preferential orientation and therefore anisotropic defect diffusion can be excluded as a major formation mechanism for elongated vacancy islands. Furthermore, the normal-incidence-sputtered surface exhibits subatomic height protrusions of nanometer dimension. These protrusions may be associated with formation of subsurface Ar bubbles due to Ar implantation. This effect also highlights that grazing ion-beam irradiation is much more surface sensitive and avoids subsurface damage and Ar accumulation and therefore is better suited for surface modifications.

With increasing ion fluences the differences in the surface morphologies for the two ion-beam azimuths become less pronounced. Figure 5 shows the evolution of the surface morphologies for "intermediate" ion fluences. Along the ⟨1$\bar{1}$0⟩ azimuth direction a transition of vacancy island shapes from "compact" to elongated islands with the long axis along the ion-beam direction is observed [Figs. 5(e) and 5(f)]. For both azimuthal directions the surface becomes rougher as vacancy islands are nucleated and grow at the bottom of previously formed vacancy islands. Importantly, however, the surface does not evolve into a randomly rough surface.

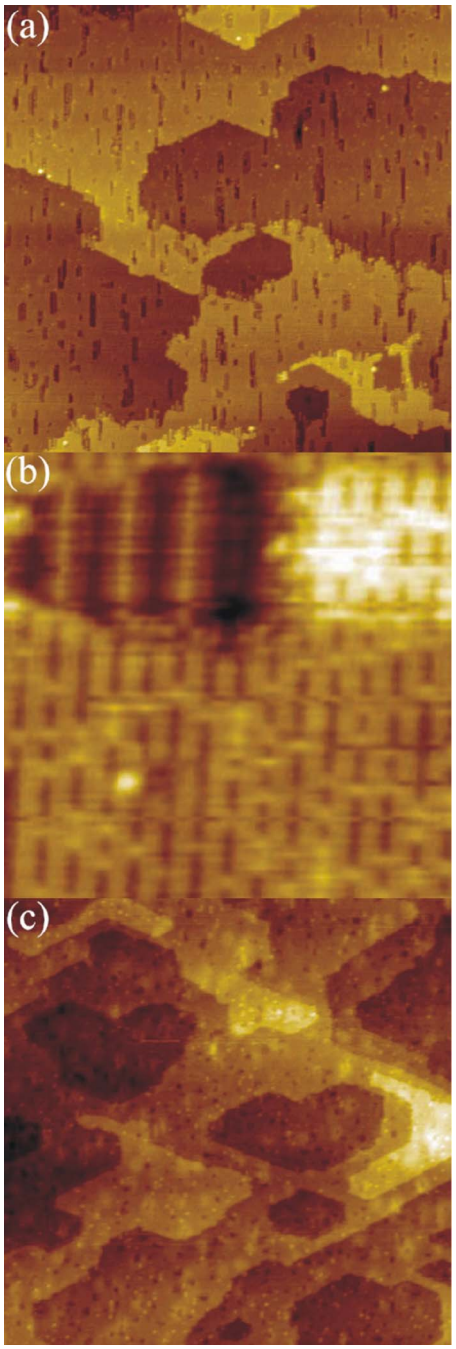

FIG. 4. (Color online) STM images of TiO_2(110) surface after various ion irradiation procedures (a) 200×200 nm^2 image after grazing ion irradiation along the ⟨001⟩ azimuth. In this image increased sputter damage on "step-up" edges is observed while steps parallel to the ion beam and "step-down" edges are not altered by the ion beam. (b) 10×10 nm^2 showing the formation of 2×1 reconstruction within the vacancy island. (c) 400×400 nm^2 image after ion irradiation at normal incidence. The formed vacancy islands do not exhibit any preferential orientation, thus excluding anisotropic vacancy island shape due to anisotropic diffusion. Also several nanometer wide subatomic height protrusions are visible which are attributed to subsurface Ar bubbles.

Instead, nanoripples with the ridges and troughs aligned in the direction of the ion beam and with a ripple separation exhibiting a characteristic separation of ~10 nm perpendicular to the ion-beam azimuth direction are formed. The ripple structures become clearly visible in Figs. 5(c) and 5(d) for the ⟨001⟩ azimuth and Figs. 5(g) and 5(h) for the ⟨1$\bar{1}$0⟩ azimuth. At lower fluences there exists no clear preferential separation between elongated vacancy islands. However, the widths of adisland and vacancy island that evolve into ridges and troughs at higher fluences have a fairly uniform characteristic width. The island widths do not change significantly throughout the surface evolution. As the surface is covered with more and more islands, the preferred width of the islands causes a close-to-uniform separation and nanoripple formation.

At the highest ion fluences used in this study, the surfaces consist of ripples with similar spacing and corrugation for the two azimuths. Representative STM images of such surfaces are shown in Fig. 6. The ⟨001⟩ azimuth appears somewhat more regular which may have its origin from the elongation of the vacancy islands from the outset of the sputtering.

V. DISCUSSION

The higher initial density of vacancy islands for ion beams impinging at the surface along the ⟨1$\bar{1}$0⟩ azimuth compared to the ⟨001⟩ azimuth suggests that the sputter yield at terraces is higher for the former. Also the strong elongation of the vacancy islands in the ion-beam direction for the ⟨001⟩ azimuth suggests that step-edge sputtering is the favored sputter mechanism.

In order to be more quantitative about the sputter yield differences for the two ion-beam orientations we estimate the number of sputtered atoms from the total vacancy island size as a function of sputter time shown in Fig. 3(c). If we differentiate between atoms sputtered from step edges and atoms sputtered from terraces the total number of sputtered atoms is given by

$$N_{\mathrm{tot}} = N_{\mathrm{step}} + N_{\mathrm{terrace}}. \quad (1)$$

The step-edge sputtering per unit area, N_{step}, is a function of the step length per unit area, which is sputter time dependent, and therefore the sputter rate (sputter yield) of the surface becomes time dependent. Figure 7(a) shows the increase in steps perpendicular to the ion beam, i.e., steps that are "exposed" to the ion beam with sputter time for the two azimuths. In this plot we only counted the step edges of vacancy islands and not the pre-existing steps at the surface. This has been done because the erosion of the pre-existing steps is difficult to evaluate from the STM images and the sputter yield is only measured from the size and density of the vacancy islands. Thus by not measuring sputtering from pre-existing steps we also must not take the length of these steps into account for evaluating the step-edge sputter yield. The estimates we obtain here are therefore consistent with hypothetical perfectly flat surfaces without any initial step edges. The increase in step-edge density for low ion fluence can be approximated with a linear increase. As the vacancy islands merge, step edges are being annihilated and the step-edge density decreases again. Therefore this analysis is only valid for short sputter times.

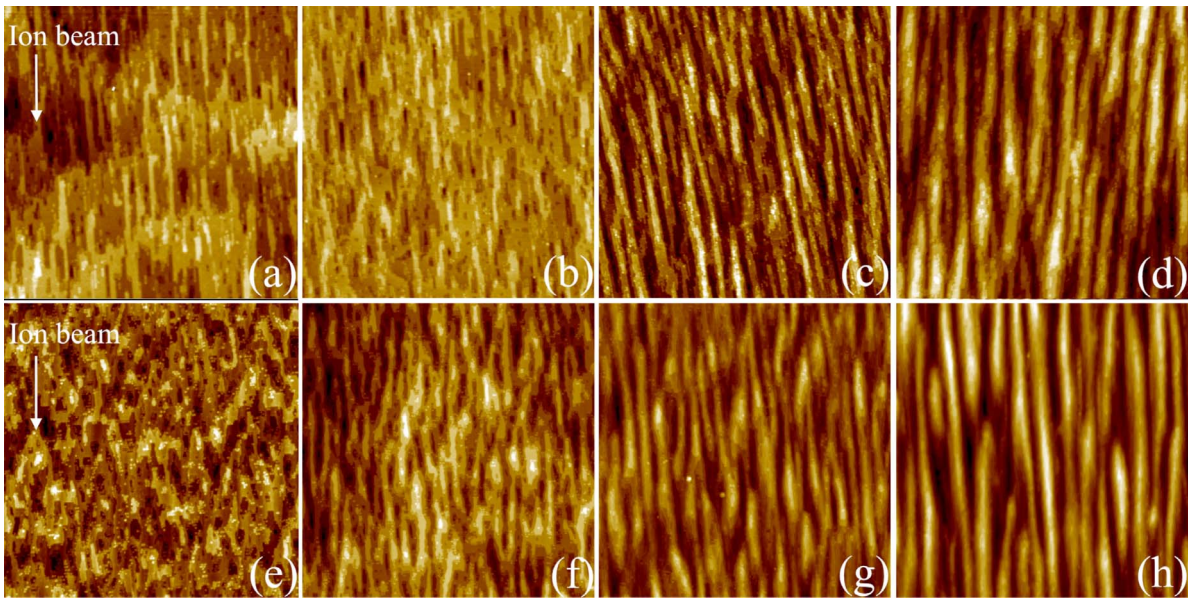

FIG. 5. (Color online) STM images of $TiO_2(110)$ (200×200 nm^2) after irradiation times of (a) 320 minutes, (b) 640 minutes, (c) 1600 minutes, and (d) 3250 minutes along the $\langle001\rangle$ azimuth, and of (e) 320 minutes, (f) 640 minutes, (g) 1600 minutes, and (h) 3250 minutes along the $\langle1\bar{1}0\rangle$ azimuth.

The number of sputtered atoms due to step-edge sputter events, N_{step}, is given by the step-edge sputter yield, Y_{step}, times the number of ions impinging in an area close to the step edge where they can induce step-edge sputtering. Thus the number of atoms sputtered from step edges per unit area can be expressed as

$$N_{step} = Y_{step} SL(t) dFt, \tag{2}$$

where $SL(t)$ is the step length per unit area [determined from Fig. 7(a)], which is a function of sputter time, d is an effective distance away from the step edge at which the impinging ions are inflicting damage at the step edge, F is the ion fluence at the surface, and t the sputter time. The effective distance, d, away from step edges is estimated from geomet-

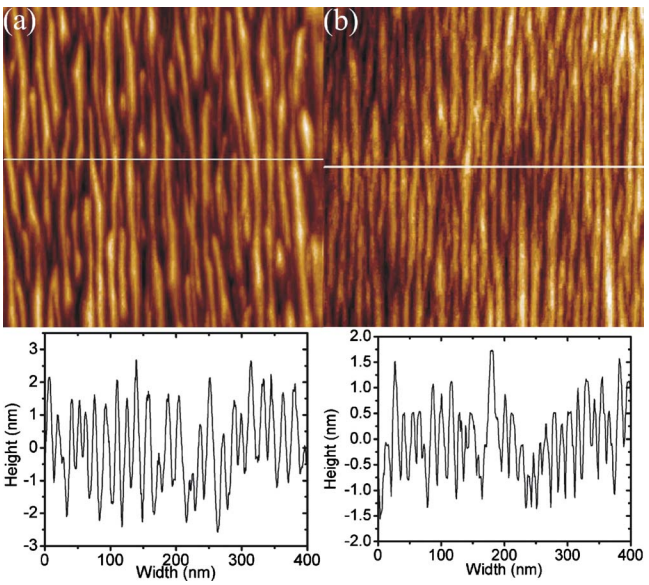

FIG. 6. (Color online) STM images (400×400 nm^2) of the surface morphology after extended periods of grazing incidence irradiation in (a) $\langle1\bar{1}0\rangle$ azimuth and (b) $\langle001\rangle$ azimuth directions. Nanoripples are formed that are aligned parallel to the ion-beam directions. The corrugation of these ripples is ~4 nm as can be judged from the shown cross-sections.

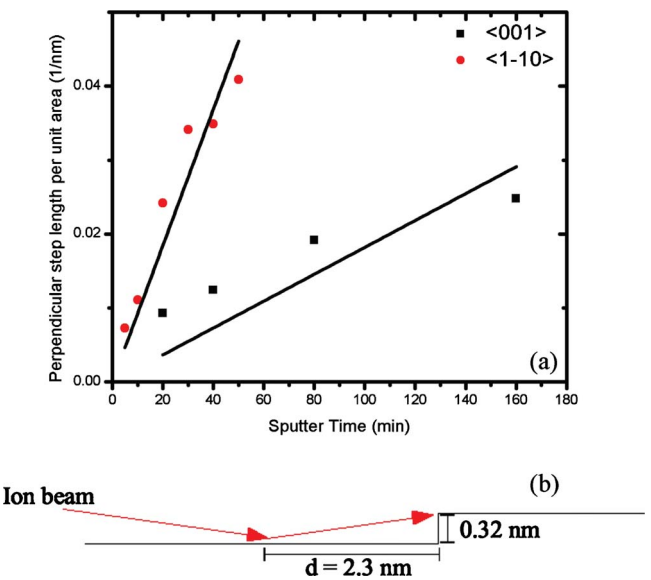

FIG. 7. (Color online) The step-edge length perpendicular to the ion beam is plotted as a function of sputter time for the $\langle001\rangle$ and the $\langle1\bar{1}0\rangle$ azimuths in (a). The lines indicate a linear fit for these data points. (b) shows the geometric argument for estimating the "effective step width," d.

TABLE I. Step edge and terrace sputter yields derived from fit to data shown in Fig. 3(c).

	Y_{step}	$Y_{terrace}$	$Y_{step}/Y_{terrace}$
⟨001⟩	0.094 ± 0.034	0.011 ± 0.002	8.5
⟨1$\bar{1}$0⟩	0.30 ± 0.072	0.014 ± 0.006	21

ric considerations as shown in Fig. 7(b). For an incidence angle of 8° and a step height of 0.32 nm a value of $d = 2.3$ nm is obtained. Estimating the change in the step length with time by a linear behavior, results in the total number of sputtered atoms from step edges to increase quadratically with sputter time. In contrast sputtering from terraces is assumed to be time independent and thus the number of sputtered atoms from terraces is given by

$$N_{terrace} = Y_{terrace} AFt, \tag{3}$$

where A is a unit-surface area. Therefore the total number of sputtered atoms is given by

$$N_{tot} = N_{step} + N_{terrace} = Y_{step} SL(t) dFt + Y_{terrace} AFt. \tag{4}$$

The total number of sputtered atoms per unit area is given by the vacancy island area [Fig. 3(c)]. A quadratic fit to the data points allows extracting the contribution from step-edge and terrace sputtering. The linear term is from terrace sputtering while the quadratic term is due to step-edge sputtering. The fitting parameters to the experimental data then enables determining of $Y_{terrace}$ by dividing the linear term by the ion fluence and unit area and Y_{step} by dividing it by $SL(t)$, d, and F, where $SL(t)$ is taken from the linear fit in Fig. 7(a). The result for the sputter yields for the two azimuths is summarized in Table I.

The ratio of step edge to terrace sputter yield is around an order of magnitude larger for both azimuth directions. Also, a higher step-edge sputter yield for the ⟨1$\bar{1}$0⟩ direction is obtained in qualitative agreement with the denser packing of step edges perpendicular to this direction as discussed above. The terrace sputter yields are the same for both azimuths within the margin of error, which contradicts our expectation of a higher terrace sputtering for the ⟨1$\bar{1}$0⟩ azimuth based on surface-structure arguments and from the experimental observation of a higher vacancy island density for low ion fluences for the ion beam directed along the ⟨1$\bar{1}$0⟩ direction compared to the ⟨001⟩ direction. This discrepancy may be ascribed to systematic errors in this analysis; such as the questionable linear dependence in the increase in the step-edge length with sputter time and the neglect of any potential influence on the sputter yield due to the formation of surface reconstruction on this particular surface. Therefore we explore an alternative for verifying the terrace sputter yield by investigating the vacancy island density at low ion fluences. Figure 3(a) indicates a roughly two to three times higher vacancy island density for the ⟨1$\bar{1}$0⟩ than for the ⟨001⟩ azimuth suggesting an also two to three times higher terrace sputter probability for the ⟨1$\bar{1}$0⟩ azimuth compared to the ⟨001⟩ azimuth. Initial nucleation of vacancy islands is due to terrace sputtering events and thus a higher vacancy island density suggests a higher terrace sputtering. Assuming a critical vacancy island size for which vacancy islands are stable of three atoms, which is the smallest vacancy island observed, allows estimating the terrace sputter yield for the two azimuths directions by the following expression:

$$Y_{terrace} = \{\text{density critical island size}\}/\{\text{ion fluence} \times \text{sputter time}\}. \tag{5}$$

With this method the terrace sputter yield is estimated to be 0.03 and 0.008 for the ⟨1$\bar{1}$0⟩ and the ⟨001⟩ azimuths, respectively. These numbers indicate a significant larger terrace sputter yield for the ⟨1$\bar{1}$0⟩ azimuth than the number derived from the quadratic fit and reconciles the surface structural argument that the terrace sputter yield should be higher with ion beam directed perpendicular to the bridging oxygen rows. Using these new values for the terrace sputter yield for restricting the linear term in the quadratic regression in Fig. 3(c) new values for the step-edge sputter yield of 0.09 and 0.14 are obtained for the ⟨1$\bar{1}$0⟩ and the ⟨001⟩ azimuths, respectively. This new fit to the experimental values is shown in Fig. 3(c) as dashed lines. Although the yields are quite different from those of the direct quadratic regression to the data points (Table I) the new quadratic fits are still close enough to the data points to be within the margin of error of the experimental data. Therefore we conclude that within the accuracy of this analysis the step-edge sputter yield is about the same for both azimuths but the terrace sputter yield varies, with approximately two to three times higher terrace sputter yield for the ⟨1$\bar{1}$0⟩ azimuth. The higher terrace sputtering along the ⟨1$\bar{1}$0⟩ direction is therefore primarily responsible for the higher total sputter yield for this azimuth direction, which causes the nucleation of more vacancy islands on terraces and thus an accelerated step-edge sputtering per unit area. This leads to the significantly larger total sputtering with the ion beam directed along the ⟨1$\bar{1}$0⟩ direction compared to the ⟨001⟩ direction as is evident from Fig. 3(c).

These variations in the terrace and step sputter yield are not sufficient to explain the strongly different vacancy island shapes for the two azimuth directions. Instead we propose that thermodynamic stability of vacancy islands play an important role in the initial shape. All the sputtering experiments have been conducted at 400 °C as a necessity to maintain crystallographic order in the surface during the experiment. In addition to short-range rearrangement of atoms, the elevated temperature also activates surface diffusion and thus the rearrangement of surface features into thermodynamically more stable configurations. In particular, undercoordinated step-edge atoms are easier rearranged than terrace or bulk atoms. This means that vacancy islands will form shapes that minimize the step-edge energies of the island. The equilibrium island shape is determined by the step-edge energies and step directions in a 2D equivalent of the Wulff construction.[34] The exact values for the step-edge energies of the TiO_2(110) surface are not known, but experimental investigations of the surface structure show that only ⟨001⟩ and {1$\bar{1}$1} step edges are present at the surface but no step edges

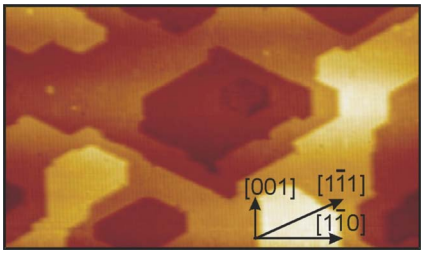

FIG. 8. (Color online) STM image of a TiO_2(110) annealed to 650 °C to form close to thermodynamic equilibrium step edges. It is apparent that only [001] and $\langle 1\bar{1}1\rangle$ step edges are present but no step edges along the $[1\bar{1}0]$ direction. This indicates that the $[1\bar{1}0]$ is an unstable step-edge orientation on TiO_2(110) surfaces.

have been observed along the $\langle 1\bar{1}0\rangle$ direction, see Fig. 8.This implies that the $\langle 1\bar{1}0\rangle$ step direction is unstable and terraces cut along this direction will rearrange to form steps with the $\{1\bar{1}1\}$ directions. In previous studies we showed that this is indeed the case, i.e., the directed ion beam can be used to stabilize steps along the $\langle 1\bar{1}0\rangle$ direction but these steps are unstable and restructure upon heat treatment[20] into the energetically favored $\{1\bar{1}1\}$ steps. This observation has implications for describing the vacancy island morphologies. For sputtering with the ion-beam azimuth along the $\langle 001\rangle$ direction, step edges parallel to the ion beam are formed by an anisotropic erosion of the surface. These $\langle 001\rangle$ step edges have a low formation energy as is evident from their presence in equilibrium island shapes. Therefore, although strongly elongated islands are not equilibrium shapes, the step edges are stable in the temperature range of the experiment. For the ion-beam direction along the $\langle 1\bar{1}0\rangle$ azimuth, on the other hand, the step edges parallel to the ion beam direction are unstable and can easily transform into $\{1\bar{1}1\}$ steps. This transformation is further aided by the small angle (24.5°) that is included between $\langle 1\bar{1}1\rangle$ and $\langle 1\bar{1}0\rangle$ crystallographic directions. Consequently, even for the grazing ion beam directed along the $\langle 1\bar{1}0\rangle$ direction small vacancy islands do not initially exhibit steps parallel to the ion beam but reorganize into vacancy islands with a more stable step-edge structure which necessarily involves formation of compact island shapes. As the vacancy islands grow in size, the $\langle 1\bar{1}0\rangle$ step edges become more frequent because it would require a larger mass transport to reshape the larger islands into equilibrium shapes. It appears that in the temperature regime and on the time scale of the experiment, there is not enough atom mobility to allow for such a significant material transport.

The ripple formation by grazing incidence ion sputtering is due to local variations in the sputter yield. Atomically flat surfaces exhibit a smaller sputter yield compared to defects, in particular, step edges under grazing incidence irradiation. This gives rise to preferential erosion of step edges that are exposed to the ion beam. As a consequence of structure-dependent sputter yield, surface features with high sputter yield are eroded faster causing self-organization of the surface into a morphology that reduces the overall sputtering. Step edges "facing" the ion beam are preferentially sputtered at the surface while step edges parallel to the ion-beam azimuth do not experience a higher erosion rate. Because sputtering at terraces is not entirely suppressed, new vacancy islands are constantly nucleated and thus a roughening of the surface is observed. As a consequence of the lower sputter yield of steps aligned parallel to the ion-beam azimuth and the tendency of surface roughening, ridges are formed that are aligned with the ion-beam azimuth. While the ion sputtering plays the central role in the alignment of the step edges parallel to the ion beam and causes surface roughening, the ion-beam effects by themselves cannot explain the formation of ripples with a characteristic separation. For this to occur, a self-regulating mechanism must be present that causes troughs to maintain a preferred separation. For nanoripple formation on metal surfaces, it has been shown that the diffusion of adatoms generated by the ion impacts plays a crucial role in regulating the ripple separation.[17] The presence of adatoms on the TiO_2 surface is not obvious, however, since excess O atoms will desorb from the surface at the temperature of the experiment and Ti adatoms are diffusing into the bulk. On the other hand, the mobility and diffusion of vacancies generated by sputtering is clearly present at the surface as is evident from the clustering of vacancies and formation of vacancy islands. Also the arrangement of vacancy islands with low-energy steps indicates step-edge diffusion. Therefore, under the experimental conditions, significant atom mobility exists at the surface. In covalent materials, step-step interactions can be strong and it has been shown, for example, for anatase TiO_2 that step separation on the order of nanometers can significantly lower the energy of stepped surfaces.[34] Repulsive step interactions would explain that vacancy and adislands always exhibit a minimum width in the STM measurements. Surfaces with enough atom mobility will arrange to lower their free energy. On a rough surface, the step-step interaction energy will contribute to the surface energy and therefore this energy contribution will regulate the average step-step separation leading to fairly uniform distribution of ripples as observed in the experiments.

Nanoripple formation by grazing incidence ion sputtering has been observed on very different materials systems, ranging from metals, to purely ionic, and now metal oxides. This indicates that the formation mechanism for ripple formation is robust. Preferential step-edge sputtering has been shown as the main mechanism responsible for directing the nanoripples in the direction of the ion-beam azimuth for all these systems. The mechanism, by which a regular pattern is formed, on the other hand, may have different origins for different systems or several mechanisms are acting together. One may differentiate self-regulating mechanisms driven by kinetics such as barriers for diffusion at step edges and other diffusion-driven mechanisms that would allow an equilibration of ripple widths, and energetic arguments that would lower the energy of the system by formation of roughly equally spaced step separation and thus cause a uniform ripple structure. In both cases, diffusion of vacancies or adatoms is crucial for establishing the ripple structure and thus the temperature can affect the ripple structures.

The fact that similar ripple structures can be formed on metals as well as on TiO_2(110) indicates that special proper-

ties of TiO_2 such as strongly anisotropic step-edge energies, easy bulk diffusion of Ti, preferential erosion of oxygen, and the directional formation of 2×1 reconstruction strands on reduced TiO_2 does not fundamentally affect the ripple-formation mechanism. Therefore, the process of grazing incidence sputtering appears to be a widely applicable method for nanopatterning of single-crystal substrate materials.

VI. CONCLUSION

Grazing incidence ion beams have been used to pattern a transition-metal oxide surface with nanoscale ripple structures by directing the ion beam along the $\langle 1\bar{1}0\rangle$ or the $\langle 001\rangle$ crystallographic directions. Ripple formation is induced by preferential step-edge sputtering by grazing incident ion beams along the low-index azimuth directions. The sputter yield was deduced from sputter-induced vacancy island sizes measured with STM as a function of ion fluence. This indicated a dependence of the sputter yield on the surface morphology under grazing incidence conditions. The dependence of the sputter yield on the step-edge density enabled a deduction of sputter yields for step edges and flat terraces. Under the ion-beam conditions used in this experiment a higher step-edge sputter yield compared to terrace sputtering has been observed for both the $\langle 1\bar{1}0\rangle$ and the $\langle 001\rangle$ azimuth directions. The terrace sputter yield appeared, however, to show a strongly azimuthal dependence which can be understood on the basis of the strongly corrugated surface structure of TiO_2(110). The directionality of the ion-beam and the higher sputter yields at step edges exposed to the ion beam causes a preferential removal of those step edges. In addition stochastic ion sputtering from terraces causes a surface roughening. These two effects combine to cause nanoripples aligned with the ion-beam azimuth. A self-regulating mechanism, such as energy minimization of step-step interaction energies, is responsible for the formation of a narrow distribution of ripple separations.

The ion-beam interaction with the surface is dominated by binary collision effects that are largely independent for the sputtered elements. Therefore this method of patterning large scale areas with nanoripples is expected to be of universal applicability if ion-beam-induced structural and compositional changes can be avoided.

ACKNOWLEDGMENT

This material is based upon work supported by the U.S. Department of Energy, Office of Basic Energy Sciences, Grant No. DE-SC0001508.

[1] A. Mathur and J. Erlebacher, Surf. Sci. **602**, 2863 (2008).
[2] J. H. Lee, D. Y. Lee, B. W. Oh, and J. H. Lee, IEEE Trans. Electron Devices **57**, 157 (2010).
[3] A. Sagar, R. M. Feenstra, C. K. Inoki, T. S. Kuan, Y. Fu, Y. T. Moon, F. Yun, and H. Morkoc, Phys. Status Solidi A **202**, 722 (2005).
[4] P. Liu, C. Lu, and Y. W. Zhang, Phys. Rev. B **76**, 085336 (2007).
[5] A. D. Brown, J. Erlebacher, W. L. Chan, and E. Chason, Phys. Rev. Lett. **95**, 056101 (2005).
[6] F. Frost, B. Ziberi, A. Schindler, and B. Rauschenbach, Appl. Phys. A: Mater. Sci. Process. **91**, 551 (2008).
[7] T. Aste and U. Valbusa, New J. Phys. **7**, 122 (2005).
[8] U. Valbusa, C. Boragno, and F. B. de Mongeot, J. Phys.: Condens. Matter **14**, 8153 (2002).
[9] S. Facsko, T. Dekorsy, C. Koerdt, C. Trappe, H. Kurz, A. Vogt, and H. L. Hartnagel, Science **285**, 1551 (1999).
[10] V. S. Smentkowski, Prog. Surf. Sci. **64**, 1 (2000).
[11] D. Danailov, J. H. Rechtien, and K. J. Snowdon, Surf. Sci. **259**, 359 (1991).
[12] K. J. Snowdon, D. J. O'Conner, and R. J. MacDonald, Phys. Rev. Lett. **61**, 1760 (1988).
[13] M. Wißing, M. Batzill, and K. J. Snowdon, Nanotechnology **8**, 40 (1997).
[14] J. Stöhr, M. G. Samant, J. Lüning, A. C. Callegari, P. Chaudhari, J. P. Doyle, J. A. Lacey, S. A. Lien, S. Purushothaman, and J. L. Speidell, Science **292**, 2299 (2001).
[15] M. Batzill, F. Bardou, and K. J. Snowdon, J. Vac. Sci. Technol. A **19**, 1829 (2001).
[16] M. Batzill, F. Bardou, and K. J. Snowdon, Phys. Rev. B **63**, 233408 (2001).
[17] H. Hansen, A. Redinger, S. Messlinger, G. Stoian, Y. Rosandi, H. M. Urbassek, U. Linke, and T. Michely, Phys. Rev. B **73**, 235414 (2006).
[18] A. Redinger, Y. Rosandi, H. M. Urbassek, and T. Michely, Phys. Rev. B **77**, 195436 (2008).
[19] H. Hansen, C. Polop, T. Michely, A. Friedrich, and H. M. Urbassek, Phys. Rev. Lett. **92**, 246106 (2004).
[20] T. Luttrell, W. K. Li, X. Q. Gong, and M. Batzill, Phys. Rev. Lett. **102**, 166103 (2009).
[21] H. Hansen, A. Redinger, S. Messlinger, G. Stoian, J. Krug, and T. Michely, Phys. Rev. Lett. **102**, 146103 (2009).
[22] S. van Dijken, D. de Bruin, and B. Poelsema, Phys. Rev. Lett. **86**, 4608 (2001).
[23] F. Krok, S. R. Saeed, Z. Postawa, and M. Szymonski, Phys. Rev. B **79**, 235432 (2009).
[24] C. C. Hsu and J. W. Rabalais, Surf. Sci. **256**, 77 (1991).
[25] Y. H. Song, Y. N. Wang, and Z. L. Miskovic, Nucl. Instrum. Methods Phys. Res. B **230**, 158 (2005).
[26] H. Bu, M. Shi, and J. W. Rabalais, Surf. Sci. **244**, 96 (1991).
[27] Y. Wang, M. Shi, and J. W. Rabalais, Nucl. Instrum. Methods Phys. Res. B **62**, 505 (1992).
[28] U. Diebold, Surf. Sci. Rep. **48**, 53 (2003).
[29] B. Hird, Can. J. Phys. **69**, 70 (1991).
[30] TRIM simulation package is available at: http://www.srim.org
[31] N. Shibata, A. Goto, S.-Y. Choi, T. Mizoguchi, S. D. Findlay, T. Yamamoto, and Y. Ikuhara, Science **322**, 570 (2008).
[32] S. D. Elliott and S. P. Bates, Phys. Chem. Chem. Phys. **3**, 1954 (2001).
[33] M. A. Henderson, Surf. Sci. **419**, 174 (1999).
[34] X. Q. Gong, M. Batzill, U. Diebold, and A. Selloni, Nature Mater. **5**, 665 (2006).